

A Simple Born-Form Approximation for $e^+e^- \rightarrow W^+W^-$ at One Loop[†]

M. Kuroda^a and D. Schildknecht^b

^a Institute of Physics, Meiji-Gakuin University
Yokohama, Japan.

^bTheory Division, CERN, Switzerland
and
Department of Theoretical Physics, University of Bielefeld
Bielefeld, Germany

Abstract

A simple Born-form approximation at the one-loop level for $e^+e^- \rightarrow W^+W^-$ at high energies is given in analytic form. The different contributions to the three invariant one-loop amplitudes, $S_I^{(-)}(s, t)$ and $S_Q^{(\pm)}(s, t)$, determining the Born-form helicity amplitudes are thoroughly investigated analytically and numerically. At energies above 500 GeV, the accuracy of the simple Born-form approximation for the differential production cross section is better than 1% for almost all W^+W^- production angles, independently of whether the W^+W^- polarization is summed over, or whether a longitudinal or a transverse polarization is selected for both the W^+ and the W^- .

[†]This work is supported partly by the Ministry of Education and Culture, Japan, under Grant-in-Aid for basic research program C (No. 08649391), by Alexander von Humboldt-Stiftung, Bonn, Germany, the BMBF, Bonn, Germany and by the EC contract CHRX-CT94-0579.

1 Introduction

The process of e^+e^- annihilation into W pairs is one of the outstanding reactions to be explored at LEP 2 and at any future linear e^+e^- collider. While simple at tree level, the evaluation of the amplitudes for this reaction at the one-loop level [1]–[3], as a consequence of the large number of contributing Feynman diagrams, leads to formulae of enormous complication only available in extensive computer codes. A simple approximation of the one-loop result, at least in the high-energy limit, is highly desirable from a theoretical point of view as well as for practical reasons.

In ref. [4], it was conjectured that the one-loop helicity amplitudes may be represented, in good approximation, by helicity amplitudes that have the form of a Born approximation, only differing from the tree-level Born amplitudes by a replacement of the electromagnetic and of the weak coupling by s - and t -dependent invariant amplitudes. The necessary condition of unitarity constraints in the high-energy limit acts as a guiding principle for the choice of the set of (only) three invariant amplitudes appearing in the Born-form approximation. In ref. [4], it was indeed shown that the total cross section and the angular distribution of the W bosons may be well approximated by such a Born-form approximation. From a slightly different point of view, an identical Born-form approximation was given in ref. [5].

The demonstration that a Born-form approximation of the helicity amplitudes is possible, in refs. [4],[5], had to rely on a numerical evaluation of the one-loop-level amplitudes. No insight into the detailed structure of the contributing three invariant amplitudes has thus been obtained, and the evaluation of the three invariant amplitudes by the corresponding computer codes is not much simpler than the evaluation of the full one-loop helicity amplitudes, which depend on twelve invariant amplitudes. In other words, the important problem of deducing a simple (high-energy) approximation for the three invariant amplitudes appearing in the Born-form approximation was left unsolved at the time. Moreover, no attempt was made in refs. [4],[5] to construct the Born-form approximation in such a manner that not only the cross section summed over W polarizations, but also the cross sections for specific W polarizations would be adequately approximated.

The purpose of the present work is twofold:

i) to show that the three invariant amplitudes appearing in the Born form for the helicity amplitudes can indeed be chosen in such a manner that the helicity amplitudes for fixed polarization of the outgoing W -bosons are adequately approximated, and

ii) to give a simple analytical high-energy approximation for these invariant amplitudes.

A realistic description[‡] of W -pair production requires that hard-photon radiation be added and W decay be taken care of in conjunction with the inclusion of background processes for which a treatment at tree level is sufficiently accurate. In this context the present work provides a simple and compact representation of the virtual electroweak and soft-photon-radiation corrections to W -pair production.

In section 2, we will give the one-loop Born form which at sufficiently high ener-

[‡] We refer to ref. [6], [7], [8] and the literature quoted therein.

gies yields an adequate approximation of the helicity amplitudes for transverse as well as longitudinal polarization of the W bosons. In section 3, a brief analytic high-energy approximation for the invariant amplitudes $S_I^{(-)}(s, t)$ and $S_Q^{(\pm)}(s, t)$ in the Born-form approximation will be given. In section 4, the simple high-energy approximation for these amplitudes will be numerically compared with the full one-loop results. In section 5, the exact and the approximated differential cross sections for various W polarizations will be compared. Some details on the derivation of the Born-form approximation described in the present paper and a numerical comparison with the previously suggested approximation are shifted to appendices A, B and C. Final conclusions will be drawn in section 6.

2 Born-Form Approximation

We briefly recall the Born approximation for the process $e^+e^- \rightarrow W^+W^-$. The helicity amplitudes may be written as a sum of two terms proportional to the squares of the SU(2) gauge coupling g and the electromagnetic coupling e :

$$\mathcal{H}(\sigma, \lambda, \bar{\lambda}) = \frac{g^2}{2} \mathcal{M}_I(\sigma, \lambda, \bar{\lambda}) \delta_{\sigma,-} + e^2 \mathcal{M}_Q(\sigma, \lambda, \bar{\lambda}). \quad (2.1)$$

Here, and elsewhere, σ and $\lambda, \bar{\lambda}$ denote twice the electron helicity and the W^+, W^- helicities, respectively. In the notation of ref. [4], the amplitudes \mathcal{M}_I and \mathcal{M}_Q are given in terms of the basic amplitudes $\bar{M}_1(\sigma, \lambda, \bar{\lambda})$ and $\bar{M}_5(\sigma, \lambda, \bar{\lambda})$ by

$$\mathcal{M}_I(\sigma, \lambda, \bar{\lambda}) = -\frac{1}{s - M_Z^2} \bar{M}_1(\sigma, \lambda, \bar{\lambda}) - \frac{1}{t} \bar{M}_5(\sigma, \lambda, \bar{\lambda}), \quad (2.2)$$

$$\mathcal{M}_Q(\sigma, \lambda, \bar{\lambda}) = \frac{M_Z^2}{s(s - M_Z^2)} \bar{M}_1(\sigma, \lambda, \bar{\lambda}). \quad (2.3)$$

The evaluation of the cross section requires a choice of the scale at which g and e are to be related to experiment. For the high-energy process of W -pair production the choice of a high-energy scale, such as the centre-of-mass energy squared s , seems most appropriate. At LEP2 energies, the choice of $s \cong M_W^2$ was shown to yield reasonable results [9]. This choice amounts to employing $e(M_W^2)$ and $g(M_W^2)$, where $g(M_W^2)$ is extracted from the theoretical value of the leptonic W^\pm -decay width Γ_ℓ^W (rather than from μ -decay) through [10]

$$g^2(M_W^2) = 48\pi \frac{\Gamma_\ell^W}{M_W} = \frac{4\sqrt{2}G_\mu M_W^2}{1 + \Delta y^{SC}}, \quad (2.4)$$

with $\Delta y^{SC} = 3.3 \times 10^{-3}$, a constant, practically independent of the values of the top-quark mass and Higgs mass, which in principle enter the radiative one-loop correction Δy^{SC} .

At the one-loop level, the helicity amplitudes depend on twelve invariant amplitudes. In the notation of ref. [4], $\mathcal{H}(\sigma, \lambda, \bar{\lambda})$ becomes

$$\mathcal{H}(\sigma, \lambda, \bar{\lambda}) = S_I^{(\sigma)} \mathcal{M}_I(\sigma, \lambda, \bar{\lambda}) + S_Q^{(\sigma)} \mathcal{M}_Q(\sigma, \lambda, \bar{\lambda}) + \sum_{i=2,3,4,6} Y_i^{(\sigma)}(s, t) \bar{M}_i(\sigma, \lambda, \bar{\lambda}), \quad (2.5)$$

with

$$S_I^{(\sigma)}(s, t) = -tY_5^{(\sigma)}(s, t), \quad (2.6)$$

$$S_Q^{(\sigma)}(s, t) = -\frac{st}{M_Z^2}Y_5^{(\sigma)}(s, t) + \frac{s(s - M_Z^2)}{M_Z^2}Y_1^{(\sigma)}(s, t). \quad (2.7)$$

We refer to ref. [4] for the explicit definition of the basic matrix elements $\bar{M}_i(\sigma, \lambda, \bar{\lambda})$. They were chosen in such a way that the invariant amplitudes $Y_i^{(\sigma)}(s, t)$ are related to various s -channel multipole interactions, a t -channel-exchange and a contact interaction.

Out of the set of twelve invariant amplitudes, only the three Born-form invariant amplitudes contain (renormalized) ultraviolet divergences and depend on an infrared cut-off. Accordingly, it was suggested in ref. [4] to approximate $\mathcal{H}(\sigma, \lambda, \bar{\lambda})$ by restricting oneself to an expression of the Born form by dropping all other terms in (2.5):

$$\mathcal{H}(\sigma, \lambda, \bar{\lambda}) = S_I^{(\sigma)}\mathcal{M}_I(\sigma, \lambda, \bar{\lambda})\delta_{\sigma,-} + S_Q^{(\sigma)}\mathcal{M}_Q(\sigma, \lambda, \bar{\lambda}). \quad (2.8)$$

We note at this point that the requirement of a Born-form approximation by itself, in general, does not uniquely determine the Born-form invariant amplitudes $S_I^{(-)}(s, t)$ and $S_Q^{(\pm)}(s, t)$. A choice of basic matrix elements different from $\bar{M}_i(\sigma, \lambda, \bar{\lambda})$, for $i = 2, 3, 4, 6$, will in general yield different invariant amplitudes, and in particular also different amplitudes $S_I^{(-)}(s, t)$ and $S_Q^{(\pm)}(s, t)$. One condition for a reasonable Born-form approximation is mandatory, however: the basic matrix elements (with the corresponding invariant amplitudes) are to be chosen in such a manner that the high-energy unitarity constraints on the helicity amplitudes are fulfilled, even upon applying the Born-form approximation (2.8). An analysis of the high-energy behaviour of the helicity amplitudes (compare [4] and table A1 in appendix A) reveals that the invariant amplitudes in the decomposition (2.5) fulfil the necessary unitarity constraints

$$S_I^{(\sigma)} \sim S_Q^{(\sigma)} \sim O(1), \quad sY_2^{(\sigma)} \sim sY_3^{(\sigma)} \sim sY_6^{(\sigma)} \sim O\left(\frac{1}{s}\right), \quad sY_4^{(\sigma)} \sim O\left(\frac{1}{s^2}\right). \quad (2.9)$$

Dropping the terms with $i = 2, 3, 4, 6$ in (2.5) thus yields a possible approximation. For transversely polarized W bosons this approximation is numerically successful; the \mathcal{M}_I term with its $1/t \sim 1/s(1 - \cos\theta)$ forward peak dominates all other contributions. For mixed W polarizations ($\lambda = 0, \bar{\lambda} = \pm 1$ and $\lambda = \pm 1, \bar{\lambda} = 0$) and for purely longitudinal polarization, this approximation turns out not to be very satisfactory.

Noting that in the high-energy limit ($\sqrt{s} \sim 2000$ GeV) the purely longitudinal amplitude becomes dominant with respect to the mixed transverse-longitudinal one [11], it is suggestive to modify the invariant amplitudes (2.6),(2.7) in the Born form (2.8) in such a manner that the purely longitudinal helicity amplitude is reproduced exactly (except for the presence of $S_I^{(+)}$), without spoiling the good approximation for the transverse case. For details we refer to appendix A, and only state the result. Choosing $S_I^{(-)}(s, t)$ as in (2.6), but modifying $S_Q^{(\pm)}(s, t)$ in (2.7) by adding an appropriate contribution containing

$Y_2^{(\sigma)}(s, t)$ and $Y_6^{(\sigma)}(s, t)$, yields the desired result, i.e.

$$S_I^{(\sigma)} = -tY_5^{(\sigma)}, \quad (2.10)$$

$$S_Q^{(\sigma)} = -\frac{st}{M_Z^2}Y_5^{(\sigma)} + \frac{s(s - M_Z^2)}{M_Z^2}[Y_1^{(\sigma)} + \frac{2}{3 - \beta^2}Y_2^{(\sigma)} + \frac{\cos^2 \theta}{3 - \beta^2}Y_6^{(\sigma)}], \quad (2.11)$$

where s is the centre-of-mass energy squared and

$$t = M_W^2 - \frac{s}{2}(1 - \beta \cos \theta) \quad \text{and} \quad \beta = \sqrt{1 - \frac{4M_W^2}{s}}. \quad (2.12)$$

Using these amplitudes at the one-loop level in the Born form (2.8) reproduces the purely longitudinal helicity amplitudes (apart from an entirely negligible contribution due to $S_I^{(+)}$), and at the same time yields an excellent high-energy approximation for the purely transverse helicities. Numerically this will be demonstrated in section 5.

We note that expression (2.11) for $S_Q^{(\pm)}(s, t)$ to be used subsequently differs from the one in ref. [4], which was motivated by unitarity considerations for the mixed polarization. In terms of $Y_i^{(\sigma)}(s, t)$ the previous approximation (compare (32) in ref. [4]) reads

$$S_I^{(\sigma)} = -tY_5^{(\sigma)}, \quad (2.13)$$

$$S_Q^{(\sigma)} = -\frac{st}{M_Z^2}Y_5^{(\sigma)} + \frac{s(s - M_Z^2)}{M_Z^2} \left[Y_1^{(\sigma)} + \frac{1}{2}Y_2^{(\sigma)} - \frac{1}{2}Y_3^{(\sigma)} - \sigma \frac{1}{2M_W^2} \cos \theta Y_4^{(\sigma)} \right]. \quad (2.14)$$

This expression is found to coincide with the so-called form-factor approximation (FFA) of ref. [5] (see also ref. [6]).

For completeness, in appendix A, we give the full expression for the helicity amplitudes, when adopting (2.10), (2.11) and (2.13), (2.14) for $S_I^{(\sigma)}(s, t)$ and $S_Q^{(\sigma)}(s, t)$. In appendix B, by evaluating $S_I^{(-)}(s, t)$ and $S_Q^{(\pm)}(s, t)$ numerically at the one-loop level, we compare the different Born-form approximations based on (2.10), (2.11) and on (2.13), (2.14) for various choices of the W^+W^- polarization. In particular in the high-energy limit ($\sqrt{s} \cong 2000$ GeV), in which purely longitudinal production (both W^+ and W^- longitudinally polarized) dominates [11] over the mixed case (one W transverse, the other one longitudinal), the novel Born-form approximation (2.10), (2.11) of the present paper yields better results than the one based on (2.13), (2.14) examined previously [4], [5], [6].

In section 3, we will give a simple analytic high-energy approximation for the invariant amplitudes $S_I^{(-)}(s, t)$ and $S_Q^{(\pm)}(s, t)$ in (2.10), (2.11). This high-energy approximation will be numerically compared with the full one-loop results for $S_I^{(-)}(s, t)$ and $S_Q^{(\pm)}(s, t)$ from (2.10) and (2.11) in section 4.

3 Analytic High-Energy Approximation for $S_I^{(-)}(s, t)$ and $S_Q^{(\pm)}(s, t)$

The reduction of the set of twelve invariant amplitudes to a set of three invariant amplitudes in the Born-form approximation provides an important conceptual simplification.

The approach develops its full power, however, upon constructing a simple analytic high-energy approximation for these three invariant amplitudes, $S_I^{(-)}(s, t)$ and $S_Q^{(\pm)}(s, t)$ at the one-loop level.

Rescaling the invariant amplitudes by their Born value (2.1), and removing the infrared singularities by adding a soft-photon bremsstrahlung correction δ_{Br} [3], we define the amplitudes $\hat{S}_I^{(-)}(s, t)$ and $\hat{S}_Q^{(\pm)}(s, t)$:

$$\hat{S}_I^{(-)} = \frac{2}{g^2} S_I^{(-)} + \frac{1}{2} \delta_{Br}, \quad (3.1)$$

$$\hat{S}_Q^{(\pm)} = \frac{1}{e^2} S_Q^{(\pm)} + \frac{1}{2} \delta_{Br}. \quad (3.2)$$

In the subsequent discussion of the numerical evaluation of the invariant amplitudes, we use these hatted quantities, which are infrared-finite, but depend on the soft-photon cut-off ΔE . Note that at tree level, $\hat{S}_I^{(-)}(s, t) = \hat{S}_Q^{(\pm)}(s, t) = 1$.

In a first step, we approximate $S_I^{(-)}(s, t)$ and $S_Q^{(\pm)}(s, t)$ by taking into account the leading fermion-loop corrections due to the light leptons and quarks and the heavy top quark, as well as the initial state radiation (ISR) in leading-log approximation.[§] The light fermions imply replacement of $\alpha(0)$ by the running electromagnetic coupling $\alpha(s)$, while the top quark yields the well-known SU(2) breaking proportional to m_t^2 . The invariant amplitudes become

$$\hat{S}_I^{(-)} = 1 + \Delta\alpha(M_W^2) - \frac{c_W^2}{s_W^2} \Delta\rho + 0.5\Delta_{LL}(s, t), \quad (3.3)$$

$$\hat{S}_Q^{(\pm)} = 1 + \Delta\alpha(s) + 0.5\Delta_{LL}(s, t), \quad (3.4)$$

with

$$\Delta\alpha(s) = \frac{\alpha}{3\pi} \sum_f Q_f^2 \log \frac{s}{m_f^2}, \quad (3.5)$$

$$\Delta\rho = \frac{3g^2}{16\pi} \frac{m_t^2}{M_W^2}, \quad (3.6)$$

$$\begin{aligned} \Delta_{LL}(s, t) = & -\frac{\alpha}{\pi} \left[\frac{3}{2} \log \frac{m_e^2}{s} + 2 \log \frac{2\Delta E}{\sqrt{s}} \left(2 + \log \frac{m_e^2}{s} + 2 \log \frac{M_W^2 - u}{M_W^2 - t} \right. \right. \\ & \left. \left. + \frac{s - 2M_W^2}{s\beta} \log \frac{1 - \beta}{1 + \beta} \right) \right], \quad (3.7) \end{aligned}$$

where β is given by (2.12) and

$$c_W^2 = 1 - s_W^2 = \frac{M_W^2}{M_Z^2}. \quad (3.8)$$

[§]When supplemented with the Coulomb correction, this approximation coincides with the improved Born approximation (IBA) of refs. [5],[6], which is sufficiently accurate at LEP energies, provided the correction Δy^{SC} from (2.4) is introduced, [9]. Note that (3.3), apart from Δ_{LL} , amounts to nothing else but using (2.4) with $\Delta y^{SC} = 0$ for the SU(2) coupling g .

One expects that this approximation, based on fermion loops and the leading-log ISR only, will be insufficient at high energies. This will be quantitatively discussed in section 4.

In order to improve the above approximation (3.3), (3.4), bosonic contributions have to be added. As we are aiming at a high-energy approximation, we add the high-energy expansions, $S_I^{(-)dom}(s, t)$ and $S_Q^{(\pm)dom}(s, t)$, of the one-loop corrections not yet taken into account in (3.3), (3.4) to obtain

$$\hat{S}_I^{(-)} = 1 + \Delta\alpha(M_W^2) - \frac{c_W^2}{s_W^2}\Delta\rho + 0.5\Delta_{LL}(s, t) + S_I^{(-)dom}(s, t), \quad (3.9)$$

$$\hat{S}_Q^{(\pm)} = 1 + \Delta\alpha(s) + 0.5\Delta_{LL}(s, t) + S_Q^{(\pm)dom}(s, t). \quad (3.10)$$

For the determination of the explicit form of $S_I^{(-)dom}(s, t)$ and $S_Q^{(\pm)dom}(s, t)$ a high-energy approximation of the full one-loop expressions must be carried out. Fortunately, this task, which is in principle straightforward and is in practice time-consuming, can be avoided by establishing a connection between $\hat{S}_I^{(-)}(s, t)$, $\hat{S}_Q^{(\pm)}(s, t)$ and results given in the literature. In ref. [12], without providing a Born-form representation for the helicity amplitudes, the differential cross sections for various polarization states of the W bosons were given at one loop in high-energy approximation.

The argument which allows one to connect (linear combinations of) $\hat{S}_I^{(-)}(s, t)$ and $\hat{S}_Q^{(\pm)}(s, t)$ with the results on one-loop cross sections in ref. [12] is slightly different for longitudinal and transverse W polarization. As emphasized before, our choice of basic matrix elements (compare (A.1) to (A.11) and (2.10), (2.11)) is such that the helicity amplitudes for both W^+ and W^- longitudinally polarized solely depend on $S_I^{(\pm)}(s, t)$ and $S_Q^{(\pm)}(s, t)$. Accordingly, by comparing the differential cross sections in terms of $\hat{S}_I^{(\pm)}(s, t)$ and $\hat{S}_Q^{(\pm)}(s, t)$ with the high-energy approximation for the differential cross sections at the one-loop level from ref. [12], we obtain

$$2s_W^2\hat{S}_Q^{(-)} + (2c_W^2 - 1)\hat{S}_I^{(-)} = 1 + \frac{1}{2}[C_{-,L}^B + C_{-,L}^F], \quad (3.11)$$

$$\hat{S}_Q^{(+)} + \frac{2c_W^2 - 1}{2s_W^2}\hat{S}_I^{(+)} = 1 + \frac{1}{2}[C_{+,L}^B + C_{+,L}^F], \quad (3.12)$$

where the high-energy one-loop corrections to the cross sections $C_{-,L}^B(s, t)$ etc., are given in ref. [12] and will be reproduced below. For details on the derivation of (3.11), (3.12) and (3.13) below, we refer to appendix C.

For transversely polarized W bosons, the helicity amplitudes in general depend on additional invariant amplitudes besides $S_I^{(\pm)}(s, t)$ and $S_Q^{(\pm)}(s, t)$. Nevertheless, from the numerical analysis of appendix B, we know that the Born-form approximation is excellent at high energies when inserting one-loop results for the invariant amplitudes. In fact, only $S_I^{(-)}(s, t)$ appears in the high-energy approximation, thus implying (compare appendix C)

$$\hat{S}_I^{(-)} = 1 + \frac{1}{2}[C_{-,T}^B + C_{-,T}^F]. \quad (3.13)$$

In order to obtain explicit expressions for $\hat{S}_I^{(-)}$ and $\hat{S}_Q^{(\pm)}$ in the high-energy approximation, we now neglect the extremely small[¶] contribution from $\hat{S}_I^{(+)}$ in (3.12). The dominant contributions to the coefficients $C_{\pm,L}^{B/F}$, $C_{-,T}^{B/F}$ depend (quadratically or linearly) on $\log(s)$ and are given in ref. [12]^{||}. Substitution on the right-hand side in (3.11) to (3.13) and numerical evaluation shows that the main part of the full one-loop results for $\hat{S}_I^{(-)}$ and $\hat{S}_Q^{(\pm)}$ is reproduced by these leading terms in the cross-section coefficients $C_{\pm,L}^{B/F}$ and $C_{-,T}^{B/F}$. In fact, the difference between this high-energy approximation and the full one-loop results for $\hat{S}_I^{(-)}$ and $\hat{S}_Q^{(\pm)}$ is only weakly dependent on energy and on the mass of the Higgs boson for reasonable Higgs masses of $M_H = 100$ GeV to $M_H = 300$ GeV. Accordingly, the rest terms beyond the leading order may be taken care of by adding small constants, correctly adjusted in magnitude to approximate the full one-loop results for $\hat{S}_I^{(-)}$ and $\hat{S}_Q^{(\pm)}$ wherein, for definiteness, the energy is chosen as $\sqrt{s} = 2$ TeV, and the Higgs mass as $M_H = 200$ GeV. In this way, we arrive at the following results:

$$\begin{aligned}
S_I^{(-)dom} = & \frac{\alpha}{4s_W^2} \left[-\frac{1 + 2c_W^2 + 8c_W^4}{4c_W^2} \left(\log \frac{s}{M_W^2}\right)^2 + \left(4 + 2\frac{s}{u}\right) \left(\log \frac{s}{M_W^2}\right) \left(\log \frac{s}{t}\right) \right. \\
& - \left(\frac{s[s(1 - 6c_W^2) + 3t]}{4c_W^2(t^2 + u^2)} + \frac{s(1 - 6c_W^2)}{2c_W^2 u}\right) \left(\log \frac{s}{t}\right)^2 \\
& - \frac{3st}{2(t^2 + u^2)} \left(\log \frac{s}{u}\right)^2 - \frac{2s}{u} \left(\log \frac{s}{t}\right) \left(\log \frac{s}{u}\right) \\
& + \frac{3(s_W^4 + 3c_W^4)}{4c_W^2} \log \frac{s}{M_W^2} - \frac{1 - 4c_W^2 + 8c_W^4}{2c_W^2} \left(\log \frac{s}{M_W^2}\right) \left(\log c_W^2\right) \\
& + 2(1 - 2c_W^2) \left(\log \frac{t}{u}\right) \left(\log \frac{s}{M_Z^2}\right) - 2s_W^2 \left(\log \frac{t}{u}\right)^2 - 8Sp\left(-\frac{u}{t}\right) \\
& \left. - \frac{s[3s + t + 6c_W^2(s + 3t)]}{4c_W^2(t^2 + u^2)} \log \frac{s}{t} - \frac{(1 - 6c_W^2)su}{4c_W^2(t^2 + u^2)} \right] - 0.012, \quad (3.14)
\end{aligned}$$

$$\begin{aligned}
S_Q^{(-)dom} = & \frac{\alpha}{8\pi s_W^2} \left[\frac{3 - 4c_W^2 + 12c_W^4 - 16c_W^6}{4c_W^2 s_W^2} \left(\log \frac{s}{M_W^2}\right)^2 \right. \\
& + \frac{56 - 57c_W^2 + 36c_W^4 - 36c_W^6}{6c_W^2 s_W^2} \log \frac{s}{M_W^2} \\
& - (1 - 2c_W^2) \frac{2(1 - 2c_W^2)^2 + 1}{2c_W^2 s_W^2} \log c_W^2 \log \frac{s}{M_W^2} + \left(4 + 2\frac{1 - 2c_W^2}{s_W^2} \frac{s}{u}\right) \log \frac{s}{M_W^2} \log \frac{s}{t} \\
& + \frac{(1 - 2c_W^2)^3}{c_W^2 s_W^2} \left(\log \frac{u}{t}\right) \left(\log \frac{s}{M_Z^2}\right) - 2\frac{1 - 2c_W^2}{s_W^2} \frac{s}{u} \left(\log \frac{s}{t}\right) \left(\log \frac{s}{u}\right) \\
& \left. - \left[\frac{1 - 16c_W^2 + 20c_W^4}{4c_W^2 s_W^2} \frac{s}{u} + \frac{1 - 2c_W^2}{4c_W^2 s_W^2} \frac{s + 3t - 6c_W^2 s}{t^2 + u^2} \right] \left(\log \frac{s}{t}\right)^2 \right]
\end{aligned}$$

[¶]The typical magnitude of $\hat{S}_I^{(+)}$ is of order 10^{-4} .

^{||}Compare (12) of ref. [12].

$$\begin{aligned}
& -\left(\frac{1}{4c_W^2 s_W^2} \frac{s}{t} + \frac{1-2c_W^2}{2s_W^2} \frac{3st}{t^2+u^2}\right) \left(\log \frac{s}{u}\right)^2 \\
& -4s_W^2 \left(\log \frac{u}{t}\right)^2 - 16s_W^2 Sp\left(-\frac{u}{t}\right) - \frac{1-2c_W^2}{4c_W^2 s_W^2} s \frac{3s+t+6c_W^2(s+3t)}{t^2+u^2} \log \frac{s}{t} \\
& -\left[\frac{(1-2c_W^2)(1-6c_W^2)}{4c_W^2 s_W^2} \frac{su}{t^2+u^2} + \frac{3}{2} \frac{m_t^2}{s_W^2 M_W^2} \log \frac{m_t^2}{s}\right] + 0.030, \tag{3.15}
\end{aligned}$$

$$\begin{aligned}
S_Q^{(+)\text{dom}} &= \frac{\alpha}{4\pi} \left[-\frac{5s_W^4 + 3c_W^4}{4c_W^2 s_W^2} \left(\log \frac{s}{M_W^2}\right)^2 + \frac{65s_W^2 + 18c_W^4}{6c_W^2 s_W^2} \log \frac{s}{M_W^2} \right. \\
& -\frac{(1-2s_W^2)^2}{2c_W^2 s_W^2} \log c_W^2 \log \frac{s}{M_W^2} + 2\frac{1-2c_W^2}{c_W^2} \log \frac{u}{t} \log \frac{s}{M_Z^2} + \frac{s}{2c_W^2 u} \left(\log \frac{s}{t}\right)^2 \\
& \left. -\frac{s}{2c_W^2 t} \left(\log \frac{s}{u}\right)^2 - 2\left(\log \frac{u}{t}\right)^2 - 8Sp\left(-\frac{u}{t}\right) + \frac{3m_t^2}{2s_W^2 M_W^2} \log \frac{m_t^2}{s} \right] + 0.045. \tag{3.16}
\end{aligned}$$

As mentioned, the constants in (3.14) to (3.16) are adjusted such that the full one-loop results for $\hat{S}_I^{(-)}$ and $\hat{S}_Q^{(\pm)}$ evaluated for $M_H = 200$ GeV at $\sqrt{s} = 2$ TeV are well reproduced. Table 1 shows the values of the constants, if these are adjusted to $\hat{S}_I^{(-)}$ and $\hat{S}_Q^{(\pm)}$ evaluated at different values of M_H and \sqrt{s} . Table 1 demonstrates that the asymptotic region for $S_I^{(-)}$ and $S_Q^{(\pm)}$ is indeed reached at $\sqrt{s} > 2$ TeV, the dependence on M_H being weak. Using constants determined at lower energy may be useful, if a better approximation at lower energy is desired, thus effectively taking into account non-leading contributions of order $1/s$ (compare $S_Q^{(+)}$, in particular).

\sqrt{s}	500 GeV	2 TeV	20 TeV
$M_H(\text{GeV})$	$S_I^{(-)\text{dom}}(s, t)$		
100	-0.012	-0.014	-0.014
200	-0.009	-0.012	-0.011
300	-0.007	-0.009	-0.009
$M_H(\text{GeV})$	$S_Q^{(-)\text{dom}}(s, t)$		
100	0.024	0.024	0.024
200	0.030	0.030	0.030
300	0.035	0.035	0.035
$M_H(\text{GeV})$	$S_Q^{(+)\text{dom}}(s, t)$		
100	0.059	0.041	0.039
200	0.063	0.045	0.042
300	0.065	0.046	0.044

Table 1: The constants in $S_I^{(-)\text{dom}}(s, t)$ and $S_Q^{(\pm)\text{dom}}(s, t)$ adjusted such that (3.14) to (3.16) yield a good approximation of the full one-loop result for $\hat{S}_I^{(-)}(s, t)$ and $\hat{S}_Q^{(\pm)}(s, t)$ at different Higgs masses and energies.

4 Numerical Evaluation of $\hat{S}_I^{(-)}(s, t)$ and $\hat{S}_Q^{(\pm)}(s, t)$

In order to compare the various approximations for $\hat{S}_I^{(-)}(s, t)$ and $\hat{S}_Q^{(\pm)}(s, t)$ of section 3, we numerically evaluated these for the choice of two energies, $\sqrt{s} = 2000$ GeV and $\sqrt{s} = 500$ GeV.

As basic electroweak input parameters, we use the fine-structure constant α and the Z^0 and W^\pm masses M_Z and M_W . Accordingly, the coupling constants e and g are given by

$$e = \sqrt{4\pi\alpha} = 0.3028, \quad g = \frac{e}{s_W} = e \frac{M_Z}{\sqrt{M_Z^2 - M_W^2}}, \quad (4.1)$$

with [13]

$$M_Z = 91.186 \text{ GeV}, \quad M_W = 80.430 \text{ GeV}. \quad (4.2)$$

As discussed in section 3, the results are insensitive to the exact value of M_H , which is chosen as $M_H = 200$ GeV. Finally, we specify lepton and quark masses

$$\begin{aligned} m_u &= 0.041 \text{ GeV}, & m_d &= 0.041 \text{ GeV}, & m_c &= 1.5 \text{ GeV}, \\ m_s &= 0.15 \text{ GeV}, & m_t &= 175.6 \text{ GeV}, & m_b &= 4.5 \text{ GeV}, \end{aligned} \quad (4.3)$$

and the soft-photon cut-off

$$\Delta E = 0.025\sqrt{s}. \quad (4.4)$$

The numerical evaluation was carried out in three steps:

i) the full one-loop results (including soft-photon radiation) for $S_I^{(-)}(s, t)$ and $S_Q^{(\pm)}(s, t)$ from (2.10), (2.11) were numerically produced by evaluating the computer code created by one of the authors [14];**

ii) the fermion-loop approximation with ISR, (3.3), (3.4), was numerically evaluated;

iii) the full high-energy approximation based on (3.9),(3.10) and (3.14) to (3.16) was numerically evaluated.

The results of the numerical analysis are presented in fig. 1 for $S_I^{(-)}(s, t)$ and in figs. 2 and 3 for $S_Q^{(\pm)}(s, t)$.

Figure 1 shows remarkably good agreement of the high-energy approximation with the full one-loop result for $\hat{S}_I^{(-)}$, apart from a small deviation in the backward region at $\sqrt{s} = 500$ GeV. According to figs. 2 and 3, also $\hat{S}_Q^{(\pm)}(s, t)$ at $\sqrt{s} = 2000$ GeV is very well represented by the high-energy approximation, while at $\sqrt{s} = 500$ GeV, there is some departure from the full one-loop result. The discrepancy between the high-energy approximation and the full one-loop result for $\hat{S}_Q^{(+)}$ at $\sqrt{s} = 500$ GeV (see fig. 3) can be removed by using a constant of magnitude +0.063, slightly larger than the value of 0.045 that gives a good approximation at $\sqrt{s} = 2000$ GeV. Compare table 1.

**The results of ref. [14] were verified to agree with refs. [3], [5], [6].

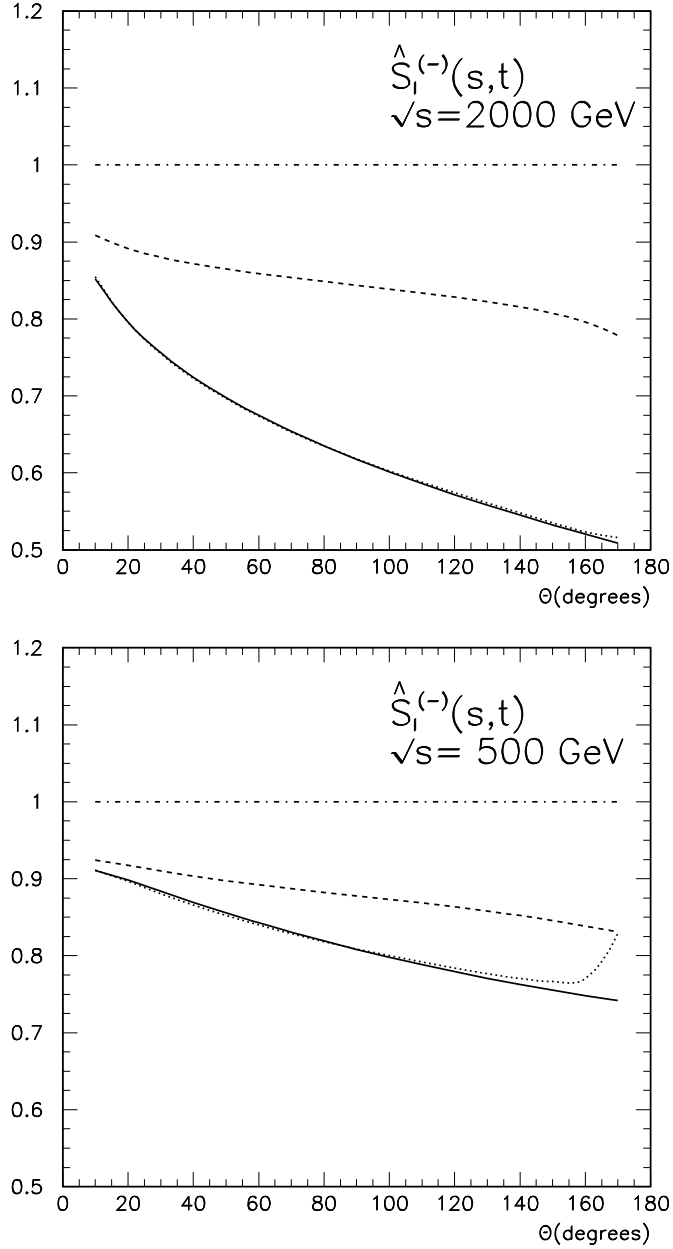


Figure 1: The Born-form invariant amplitude $\hat{S}_I^{(-)}(s,t)$ as a function of the W production angle, θ , for $\sqrt{s} = 2000$ GeV and $\sqrt{s} = 500$ GeV in (i) the full one-loop evaluation including soft-photon bremsstrahlung (solid line), (ii) the fermion-loop approximation including soft-photon bremsstrahlung (dashed line), (iii) the high-energy approximation based on (3.9),(3.10) and (3.14) to (3.16)(dotted line), (iv) the Born approximation (dash-dotted line).

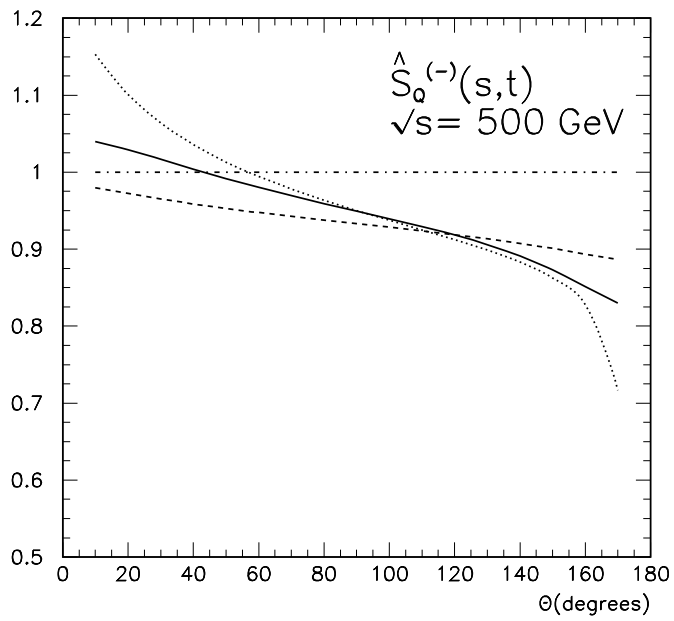
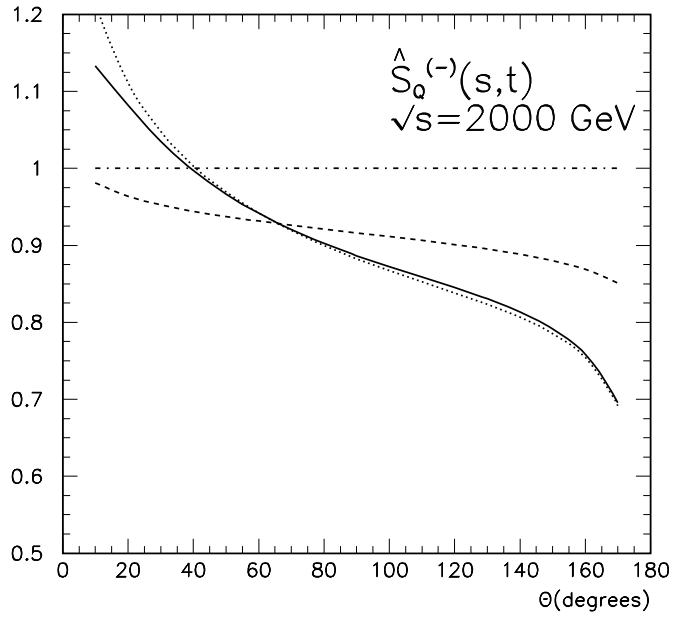


Figure 2: Same as fig.1, but for $\hat{S}_Q^{(-)}(s,t)$

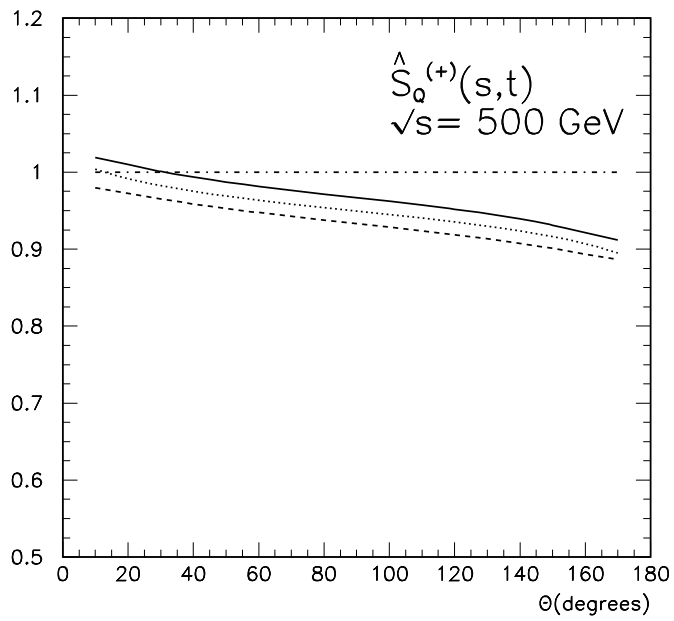
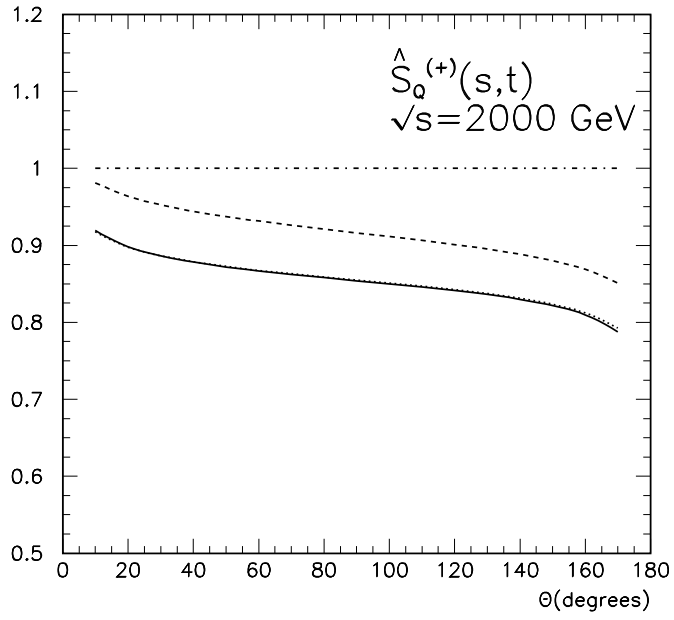


Figure 3: Same as fig.1, but for $\hat{S}_Q^{(+)}(s,t)$

It is worth stressing the large difference in $\hat{S}_I^{(-)}(s, t)$ and $\hat{S}_Q^{(\pm)}(s, t)$, particularly at 2000 GeV, between the fermion-loop approximation with leading-log ISR, (3.3),(3.4) and the full one-loop result or, equivalently, the high-energy approximation based on (3.9) and (3.10) upon substituting (3.14) to (3.16). As the soft-photon cut-off ΔE drops out of the difference between the fermion-loop approximation with leading-log ISR and the full one-loop results (or the high-energy approximation), the large difference between the corresponding curves in figs. 1 to 3 constitutes a genuine effect of virtual electroweak radiative corrections. This effect of, e.g., 10% to 30% in $\hat{S}_I^{(-)}(s, t)$ at $\sqrt{s} = 2000$ GeV, is independent of the Higgs-boson mass, but it constitutes a genuine effect due to the non-Abelian form of the electroweak theory, which gives rise to various box diagrams and vertex corrections of bosonic origin.

In section 2 and appendix A, we pointed out that $S_I^{(-)}(s, t)$ and $S_Q^{(\pm)}(s, t)$ from (2.10), (2.11), evaluated at one-loop level, yield an excellent (Born-form) approximation of the differential cross sections for various W polarizations in the high-energy limit. Since $S_I^{(-)}(s, t)$ and $S_Q^{(\pm)}(s, t)$ at one loop are well approximated by the simple high-energy form (3.9), (3.10), we expect excellent results for differential cross sections when employing (3.9), (3.10). The detailed numerical investigation of various differential cross sections is the subject of section 5.

5 Numerical Results for Differential Cross Sections, including W -Polarization

In this section, we will present a detailed comparison of the numerical results obtained for various differential cross sections at $\sqrt{s} = 2000$ GeV and at $\sqrt{s} = 500$ GeV in

- i) the full one-loop evaluation, generated by the computer code of ref. [14],
- ii) the Born-form approximation, using the exact one-loop expressions for $S_I^{(-)}(s, t)$ and $S_Q^{(\pm)}(s, t)$ generated by the computer code of ref. [14],
- iii) the high-energy Born-form approximation with $S_I^{(-)}(s, t)$ and $S_Q^{(\pm)}(s, t)$ evaluated in the high-energy approximation (3.9), (3.10) upon substituting (3.14) to (3.16).

The accuracy of a specific approximation will be quantified by the percentage deviation

$$\Delta(\%) \equiv \frac{d\sigma_{approx.} - d\sigma_{full\ one-loop}}{d\sigma_{Born}}, \quad (5.1)$$

which is obviously independent of the arbitrary soft-photon cut-off ΔE .

First of all, we concentrate on the total cross sections for fixed polarization of the produced W bosons. Table 2 shows, for $\sqrt{s} = 2000$ GeV and $\sqrt{s} = 500$ GeV, the cross section summed over the polarization of the W bosons (“unpolarized”) as well as the cross sections for the cases where both the W^+ and the W^- are transversely and longitudinally polarized, and, finally, the cross section for the case of one longitudinally and one transversely polarized W (“mixed”). One observes that there is no significant difference

	High-energy Born-form approximation		Born-form approximation		Full one-loop	Born
	$\sigma(\text{pb})$	$\Delta(\%)$	$\sigma(\text{pb})$	$\Delta(\%)$	$\sigma(\text{pb})$	$\sigma(\text{pb})$
$\sqrt{s} = 2000 \text{ GeV}$						
“Unpol.”	1.461×10^{-1}	+0.14	1.461×10^{-1}	+0.16	1.457×10^{-1}	2.758×10^{-1}
Transv.	1.422×10^{-1}	+0.19	1.423×10^{-1}	+0.19	1.417×10^{-1}	2.683×10^{-1}
Longit.	3.524×10^{-3}	-0.13	3.533×10^{-3}	0.00	3.533×10^{-3}	6.788×10^{-3}
Mixed	2.911×10^{-4}	-14.80	2.909×10^{-4}	-14.83	3.833×10^{-4}	6.229×10^{-4}
$\sqrt{s} = 500 \text{ GeV}$						
“Unpol.”	3.448	-0.42	3.462	-0.11	3.467	4.545
Transv.	3.260	-0.34	3.274	-0.01	3.274	4.294
Longit.	8.284×10^{-2}	-0.36	8.323×10^{-2}	0.00	8.323×10^{-2}	1.091×10^{-1}
Mixed	1.033×10^{-1}	-3.19	1.034×10^{-1}	-3.13	1.078×10^{-1}	1.419×10^{-1}

Table 2: The total cross section for W pair production (obtained by integration over the angular range of the production angle of $10^\circ \leq \vartheta \leq 170^\circ$) at $\sqrt{s} = 2000 \text{ GeV}$ and $\sqrt{s} = 500 \text{ GeV}$. Rows show the results when summing over the W^+W^- spins (“unpol.”) and the results for the various cases of polarization of the produced W^+ and W^- . The first column shows the result of the Born-form approximation using the high-energy approximation for $S_I^{(-)}$ and $S_Q^{(\pm)}$ given by (3.9) and (3.10) with (3.14) to (3.16). The second column gives the result of the Born-form approximation obtained by evaluating (2.10) and (2.11) at the one-loop level exactly. The third column shows the full one-loop result and the Born approximation.

between the high-energy Born-form approximation (iii) and the Born-form approximation (ii) in all these cases. For the unpolarized, transverse and longitudinal cases, the accuracy of the Born-form approximation, with $\Delta < 0.5\%$, is truly excellent. As the mixed polarization at $\sqrt{s} = 2000 \text{ GeV}$ contributes only a tiny fraction of about 2 per mille to the cross section, the fairly large deviation between the Born-form approximation and the full one-loop results is irrelevant with respect to future experiments. At $\sqrt{s} = 500 \text{ GeV}$, the mixed case contributes about 3% percent to the cross section, and an accuracy of 3% is therefore sufficient.

A detailed analysis of the differential cross sections at $\sqrt{s} = 2000 \text{ GeV}$ and at $\sqrt{s} = 500 \text{ GeV}$ for various polarization states of the W -bosons is presented in tables 3 and 4, respectively. For the W^\pm -spin-summed, transverse and longitudinal cases, the accuracy of the high-energy Born-form approximation at $\sqrt{s} = 2000 \text{ GeV}$ is better than 1%, except for the production angle of 170° , where the accuracy is of order 3%. Even at $\sqrt{s} = 500 \text{ GeV}$, the accuracy of the high-energy Born-form approximation stays below 1% for most of the angular range. For the case of mixed polarizations, because of the strong suppression of the cross section relative to the sum of purely longitudinal and transverse production, at $\sqrt{s} = 2000 \text{ GeV}$, the larger deviations in the Born-form approximation are fairly irrelevant, not only for the total but also for the differential cross section. At $\sqrt{s} = 500 \text{ GeV}$, the relative contribution of the mixed polarization is larger than in the asymptotic

angle ($^\circ$)	High-energy Born-form approximation		Born-form approximation		Full one-loop	Born
	$\frac{d\sigma}{d\cos\theta}$ (pb)	Δ (%)	$\frac{d\sigma}{d\cos\theta}$ (pb)	Δ (%)	$\frac{d\sigma}{d\cos\theta}$ (pb)	$\frac{d\sigma}{d\cos\theta}$ (pb)
	$\sigma^{\text{"unpol"}}$					
10	3.785	+0.66	3.751	+0.02	3.750	5.329
30	2.588×10^{-1}	+0.04	2.599×10^{-1}	+0.26	2.586×10^{-1}	5.070×10^{-1}
50	5.511×10^{-2}	+0.08	5.551×10^{-2}	+0.37	5.500×10^{-2}	1.382×10^{-1}
70	1.717×10^{-2}	+0.02	1.727×10^{-2}	+0.21	1.716×10^{-2}	5.208×10^{-2}
90	7.570×10^{-3}	-0.08	7.565×10^{-3}	-0.10	7.592×10^{-3}	2.605×10^{-2}
110	4.104×10^{-3}	-0.19	4.074×10^{-3}	-0.38	4.135×10^{-3}	1.599×10^{-2}
130	2.034×10^{-3}	-0.20	2.007×10^{-3}	-0.49	2.053×10^{-3}	9.466×10^{-3}
150	6.720×10^{-4}	+0.11	6.589×10^{-4}	-0.22	6.678×10^{-4}	3.993×10^{-3}
170	8.182×10^{-5}	+2.79	7.567×10^{-5}	+1.76	6.520×10^{-5}	5.961×10^{-4}
	σ_T					
10	3.784	+0.66	3.751	+0.04	3.749	5.329
30	2.574×10^{-1}	+0.08	2.585×10^{-1}	+0.30	2.570×10^{-1}	5.050×10^{-1}
50	5.290×10^{-2}	+0.15	5.330×10^{-2}	+0.45	5.270×10^{-2}	1.347×10^{-1}
70	1.445×10^{-2}	+0.17	1.454×10^{-2}	+0.36	1.437×10^{-2}	4.720×10^{-2}
90	4.891×10^{-3}	+0.07	4.875×10^{-3}	-0.00	4.876×10^{-3}	2.072×10^{-2}
110	1.998×10^{-3}	-0.11	1.956×10^{-3}	-0.48	2.010×10^{-3}	1.135×10^{-2}
130	7.747×10^{-4}	-0.25	7.400×10^{-4}	-0.80	7.907×10^{-4}	6.367×10^{-3}
150	1.837×10^{-4}	-0.19	1.689×10^{-4}	-0.76	1.887×10^{-4}	2.603×10^{-3}
170	9.944×10^{-6}	+1.18	5.448×10^{-6}	-0.26	6.262×10^{-6}	3.124×10^{-4}
	σ_L					
10	4.644×10^{-5}	+7.71	4.329×10^{-5}	0.00	4.329×10^{-5}	4.084×10^{-5}
30	8.995×10^{-4}	+0.88	8.894×10^{-4}	0.00	8.894×10^{-4}	1.146×10^{-3}
50	1.917×10^{-3}	+0.07	1.915×10^{-3}	0.00	1.915×10^{-3}	2.917×10^{-3}
70	2.574×10^{-3}	-0.13	2.580×10^{-3}	0.00	2.580×10^{-3}	4.487×10^{-3}
90	2.614×10^{-3}	-0.21	2.625×10^{-3}	0.00	2.625×10^{-3}	5.126×10^{-3}
110	2.074×10^{-3}	-0.24	2.085×10^{-3}	0.00	2.085×10^{-3}	4.546×10^{-3}
130	1.229×10^{-3}	-0.23	1.236×10^{-3}	0.00	1.236×10^{-3}	3.028×10^{-3}
150	4.512×10^{-3}	-0.12	4.528×10^{-4}	+0.01	4.527×10^{-4}	1.292×10^{-3}
170	3.925×10^{-5}	+0.55	3.834×10^{-5}	-0.04	3.840×10^{-5}	1.559×10^{-4}
	σ_{mixed}					
10	6.644×10^{-4}	-36.56	6.425×10^{-4}	-39.22	9.655×10^{-4}	8.236×10^{-4}
30	4.956×10^{-4}	-19.56	4.946×10^{-4}	-19.68	6.608×10^{-4}	8.444×10^{-4}
50	2.948×10^{-4}	-15.15	2.959×10^{-4}	-14.97	3.907×10^{-4}	6.332×10^{-4}
70	1.493×10^{-4}	-13.83	1.500×10^{-4}	-13.65	2.037×10^{-4}	3.933×10^{-4}
90	6.524×10^{-5}	-13.14	6.528×10^{-5}	-13.12	9.151×10^{-5}	1.999×10^{-4}
110	3.254×10^{-5}	-8.12	3.252×10^{-5}	-10.57	4.010×10^{-5}	9.307×10^{-5}
130	3.065×10^{-5}	+5.86	3.082×10^{-5}	+6.10	2.649×10^{-5}	7.099×10^{-5}
150	3.707×10^{-5}	+10.89	3.723×10^{-5}	+11.05	2.638×10^{-5}	9.818×10^{-5}
170	3.262×10^{-5}	+9.45	3.188×10^{-5}	+8.87	2.054×10^{-5}	1.278×10^{-4}

Table 3: The differential cross section for $e^+e^- \rightarrow W^+W^-$ at $\sqrt{s} = 2000$ GeV for various polarization states of the W^+ and W^- . The first column shows the Born-form approximation, using the high-energy approximation for $S_I^{(-)}(s, t)$ and $S_Q^{(\pm)}(s, t)$ from (3.9), (3.10) with (3.14) to (3.16). The second column is based on an exact one-loop evaluation of $S_I^{(-)}(s, t)$ and $S_Q^{(\pm)}(s, t)$ from (2.10), (2.11). The third and fourth columns show full one-loop results and the Born approximation, respectively.

angle ($^{\circ}$)	High-energy Born-form approximation		Born-form approximation		Full one-loop	Born
	$\frac{d\sigma}{d\cos\theta}$ (pb)	Δ (%)	$\frac{d\sigma}{d\cos\theta}$ (pb)	Δ (%)	$\frac{d\sigma}{d\cos\theta}$ (pb)	$\frac{d\sigma}{d\cos\theta}$ (pb)
	$\sigma^{\text{“unpol”}}$					
10	6.166×10^1	+0.04	6.164×10^1	+0.01	6.163×10^1	7.502×10^1
30	6.475	-0.65	6.524	-0.07	6.530	8.495
50	1.725	-0.86	1.740	-0.25	1.746	2.432
70	6.441×10^{-1}	-0.75	6.474×10^{-1}	-0.41	6.513×10^{-1}	9.578×10^{-1}
90	3.158×10^{-1}	-0.41	3.158×10^{-1}	-0.41	3.178×10^{-1}	4.868×10^{-1}
110	1.869×10^{-1}	-0.03	1.861×10^{-1}	-0.30	1.870×10^{-1}	2.974×10^{-1}
130	1.108×10^{-1}	+0.44	1.099×10^{-1}	-0.05	1.100×10^{-1}	1.824×10^{-1}
150	5.599×10^{-2}	+1.56	5.507×10^{-2}	+0.58	5.452×10^{-2}	9.418×10^{-2}
170	2.534×10^{-2}	+3.95	2.434×10^{-1}	+1.55	2.369×10^{-2}	4.182×10^{-2}
	σ_T					
10	6.131×10^1	+0.04	6.128×10^1	+0.00	6.128×10^1	7.457×10^1
30	6.340	-0.59	6.390	+0.00	6.389	8.329
50	1.585	-0.67	1.600	+0.00	1.600	2.250
70	5.203×10^{-1}	-0.39	5.232×10^{-1}	-0.02	5.234×10^{-1}	7.915×10^{-1}
90	2.153×10^{-1}	+0.09	2.149×10^{-1}	-0.03	2.150×10^{-1}	3.484×10^{-1}
110	1.117×10^{-1}	+0.37	1.105×10^{-1}	-0.26	1.110×10^{-1}	1.914×10^{-1}
130	5.960×10^{-2}	+0.62	5.835×10^{-2}	-0.54	5.893×10^{-2}	1.077×10^{-1}
150	2.350×10^{-2}	+1.85	2.251×10^{-2}	-0.54	2.274×10^{-2}	4.408×10^{-2}
170	3.486×10^{-3}	+17.29	2.561×10^{-3}	-0.21	2.571×10^{-3}	5.293×10^{-3}
	σ_L					
10	1.417×10^{-1}	-1.02	1.435×10^{-1}	0.00	1.435×10^{-1}	1.772×10^{-1}
30	3.119×10^{-3}	-5.43	3.309×10^{-3}	0.00	3.309×10^{-3}	3.497×10^{-3}
50	2.620×10^{-2}	+0.73	2.599×10^{-2}	0.00	2.599×10^{-2}	2.869×10^{-2}
70	5.367×10^{-2}	-0.12	5.375×10^{-2}	0.00	5.375×10^{-2}	6.543×10^{-2}
90	6.597×10^{-2}	-0.43	6.634×10^{-2}	0.00	6.634×10^{-2}	8.630×10^{-2}
110	5.900×10^{-2}	-0.44	5.939×10^{-2}	0.00	5.939×10^{-2}	8.185×10^{-2}
130	3.847×10^{-2}	-0.48	3.866×10^{-2}	-0.020	3.867×10^{-2}	5.647×10^{-2}
150	1.571×10^{-2}	+0.00	1.570×10^{-2}	-0.04	1.571×10^{-2}	2.454×10^{-2}
170	1.789×10^{-3}	+0.77	1.763×10^{-3}	-0.10	1.766×10^{-3}	2.986×10^{-3}
	σ_{mixed}					
10	2.086×10^{-1}	+1.29	2.158×10^{-1}	+3.94	2.051×10^{-1}	2.714×10^{-1}
30	1.318×10^{-1}	-3.82	1.310×10^{-1}	-4.31	1.380×10^{-1}	1.625×10^{-1}
50	1.142×10^{-1}	-3.98	1.144×10^{-1}	-3.85	1.203×10^{-1}	1.531×10^{-1}
70	7.017×10^{-2}	-3.93	7.041×10^{-2}	-3.69	7.413×10^{-2}	1.008×10^{-1}
90	3.459×10^{-2}	-3.59	3.462×10^{-2}	-3.53	3.646×10^{-2}	5.216×10^{-2}
110	1.614×10^{-2}	-1.86	1.616×10^{-2}	-1.78	1.659×10^{-2}	2.414×10^{-2}
130	1.276×10^{-2}	+1.86	1.286×10^{-2}	+2.41	1.242×10^{-2}	1.825×10^{-2}
150	1.678×10^{-2}	+2.78	1.686×10^{-2}	+3.09	1.607×10^{-2}	2.556×10^{-2}
170	2.006×10^{-2}	+2.12	2.002×10^{-2}	+2.00	1.935×10^{-2}	3.355×10^{-2}

Table 4: Same as table 3, but for $\sqrt{s} = 500$ GeV.

region of $\sqrt{s} = 2000$ GeV, but the accuracy of the approximation, of order 3%, is also substantially better.

In summary, the high-energy Born-form approximation described in the present paper provides, in general, a fully satisfactory description of the differential production cross section for various polarization states of the W -bosons at the one-loop level. We stress again the simplicity of the underlying one-loop high-energy approximation based on formulae that roughly fill a single page in section 3, while the complete expressions need a factor of 10 to 100 more space [2], [3], [14].

6 Conclusion

It has been known for some time that a Born-form approximation with three invariant amplitudes yields a satisfactory approximation of the differential cross section for W -pair production at one loop. In this paper, we present a novel choice for the one-loop invariant amplitudes that is well suited for an approximation in the high-energy limit, including W polarization. The invariant amplitudes, $S_I^{(-)}(s, t)$ and $S_Q^{(\pm)}(s, t)$, replace the weak and electromagnetic couplings appearing at tree level, and their high-energy form can be written down in a few lines. It is worth stressing that a dominant and fairly big contribution to the invariant amplitudes at high energies is of genuine electroweak origin. This dominant part is due to (non-Abelian) bosonic loops, but it is fairly insensitive to the value of the Higgs mass, as long as the Higgs mass is constrained to values for which perturbation theory provides a good approximation.

Acknowledgement

It is a pleasure to thank Stefan Dittmaier for useful discussions.

Appendix A. Helicity Amplitudes and High-Energy Behaviour

In this appendix we briefly recall the origin of the unitarity constraints (2.9). Furthermore, we give the helicity amplitudes in the representations that yield the Born-form amplitudes (2.10), (2.11) and (2.13), (2.14), respectively.

The unitarity constraints (2.9) on the invariant amplitudes follow from inspection of table A1, which shows the high-energy approximation of the basic matrix elements, $\mathcal{M}_I^{(\sigma)}$, $\mathcal{M}_Q^{(\sigma)}$ and $\bar{M}_i^{(\sigma)}$ ($i = 2, 3, 4, 6$). The requirement of a unitarity-preserving high-energy behaviour of the helicity amplitudes, together with the linear independence of the column vectors of the matrix in table A1, implies the high-energy constraints (2.9).

$(\sigma; \lambda, \bar{\lambda})$	\mathcal{M}_I	\mathcal{M}_Q	$\frac{1}{s}\bar{M}_2$	$\frac{1}{s}\bar{M}_3$
$(\pm; 00)$	$\frac{1-2c_W^2}{\sqrt{2}c_W^2}$	$-\frac{1}{\sqrt{2}c_W^2}$	$-\frac{s}{\sqrt{2}M_W^2}$	0
$(\pm; --)(\pm; ++)$	$\sqrt{2}\frac{M_W^2}{s}\left[\frac{1-4c_W^2}{c_W^2} + \frac{2}{1-\cos\theta}\right]$	$-\sqrt{2}\frac{M_Z^2}{s}$	0	$\frac{s}{\sqrt{2}M_W^2}$
$(\pm; \mp\pm)$	$\frac{2}{1-\cos\theta}$	0	0	0
$(\pm; \pm\mp)$	$\frac{2}{1-\cos\theta}$	0	0	0
$(+; -0)(+; 0+)$ $(- : 0-)(-; +0)$	$\frac{2M_W}{\sqrt{2}s}\left[\frac{1-4c_W^2}{c_W^2} + \frac{4}{1-\cos\theta}\right]$	$-\frac{2M_W}{\sqrt{2}sc_W^2}$	$-\frac{\sqrt{s}}{\sqrt{2}M_W}$	$\frac{\sqrt{s}}{\sqrt{2}M_W}$
$(+; 0-)(+; +0)$ $(- : -0)(-; 0+)$	$\frac{2M_W}{\sqrt{2}s}\left[\frac{1}{c_W^2} - 4\right]$	$-\frac{2M_W}{\sqrt{2}sc_W^2}$	$-\frac{\sqrt{s}}{\sqrt{2}M_W}$	$\frac{\sqrt{s}}{\sqrt{2}M_W}$

$(\sigma; \lambda, \bar{\lambda})$	$\frac{1}{s}\bar{M}_4$	$\frac{1}{s}\bar{M}_6$	$d_{\Delta\sigma, \Delta\lambda}^{J_0}$
$(\pm; 00)$	0	$-\frac{s}{M_W^2}\frac{\cos^2\theta}{2\sqrt{2}}$	$\mp\frac{\sin\theta}{\sqrt{2}}$
$(\pm; --)(\pm; ++)$	0	$\frac{\sin^2\theta}{\sqrt{2}}$	$\mp\frac{\sin\theta}{\sqrt{2}}$
$(\pm; \mp\pm)$	0	$-(1 + \cos\theta)$	$\mp(1 - \cos\theta)\frac{\sin\theta}{2}$
$(\pm; \pm\mp)$	0	$1 - \cos\theta$	$\pm(1 + \cos\theta)\frac{\sin\theta}{2}$
$(+; -0)(+; 0+)$ $(- : 0-)(-; +0)$	$-\sigma\frac{\sqrt{s}}{\sqrt{2}M_WM_W^2}$	$-\frac{\sqrt{s}}{\sqrt{2}M_W}(1 + \cos\theta)\cos\theta$	$\frac{1}{2}(1 - \cos\theta)$
$(+; 0-)(+; +0)$ $(- : -0)(-; 0+)$	$\sigma\frac{\sqrt{s}}{\sqrt{2}M_WM_W^2}$	$\frac{\sqrt{s}}{\sqrt{2}M_W}(1 - \cos\theta)\cos\theta$	$\frac{1}{2}(1 + \cos\theta)$

Table A1. The high-energy behaviour of \mathcal{M}_I , \mathcal{M}_Q and $\frac{1}{s}\bar{M}_i$, which is obtained by multiplying each entry by the factor $d_{\Delta\sigma, \Delta\lambda}^{J_0}$ given in the rightmost column.

We turn to the helicity amplitudes in a representation that contains the Born form (2.8) with $S_I^{(\sigma)}(s, t)$ and $S_Q^{(\sigma)}(s, t)$ from (2.10), (2.11) as an approximation. The helicity amplitudes (2.5) may in fact be rewritten identically in the form

$$\mathcal{H}(\sigma, \lambda, \bar{\lambda}) = S_I^{(\sigma)}(s, t)\mathcal{M}_I(\sigma, \lambda, \bar{\lambda}) + S_Q^{(\sigma)}(s, t)\mathcal{M}_Q(\sigma, \lambda, \bar{\lambda}) + \sum_{i=3}^6 S_i^{(\sigma)}(s, t)\mathcal{M}_i(\sigma, \lambda, \bar{\lambda}), \quad (\text{A.1})$$

with $S_I^{(\sigma)}(s, t)$ and $S_Q^{(\sigma)}(s, t)$ in the form (2.10), (2.11), i.e.

$$S_I^{(\sigma)} = -tY_5^{(\sigma)}, \quad (\text{A.2})$$

$$S_Q^{(\sigma)} = -\frac{st}{M_Z^2}Y_5^{(\sigma)} + \frac{s(s - M_Z^2)}{M_Z^2}[Y_1^{(\sigma)} + \frac{2}{3 - \beta^2}Y_2^{(\sigma)} + \frac{\cos^2 \theta}{3 - \beta^2}Y_6^{(\sigma)}], \quad (\text{A.3})$$

and

$$S_3^{(\sigma)} = sY_2^{(\sigma)}, \quad (\text{A.4})$$

$$S_4^{(\sigma)} = sY_3^{(\sigma)}, \quad (\text{A.5})$$

$$S_5^{(\sigma)} = sY_4^{(\sigma)}, \quad (\text{A.6})$$

$$S_6^{(\sigma)} = sY_6^{(\sigma)}, \quad (\text{A.7})$$

with

$$\mathcal{M}_3 = \frac{1}{s}\bar{M}_2 - \frac{s - M_Z^2}{M_Z^2} \frac{2}{3 - \beta^2}\mathcal{M}_Q = \frac{1}{s}\bar{M}_2 - \frac{1}{s} \frac{2}{3 - \beta^2}\bar{M}_1, \quad (\text{A.8})$$

$$\mathcal{M}_4 = \frac{1}{s}\bar{M}_3, \quad (\text{A.9})$$

$$\mathcal{M}_5 = \frac{1}{s}\bar{M}_4, \quad (\text{A.10})$$

$$\mathcal{M}_6 = \frac{1}{s}\bar{M}_6 - \frac{s - M_Z^2}{M_Z^2} \frac{\cos^2 \theta}{3 - \beta^2}\mathcal{M}_Q = \frac{1}{s}\bar{M}_6 - \frac{1}{s} \frac{\cos^2 \theta}{3 - \beta^2}\bar{M}_1. \quad (\text{A.11})$$

In this basis, $\mathcal{M}_i(\sigma, \lambda = \bar{\lambda} = 0) = 0$ for $i = 3, 4, 5, 6$; the longitudinal helicity amplitudes reduce to the Born form, except for the presence of $S_I^{(+)}$ which at one loop turns out to be suppressed by several orders of magnitude relative to the other Born-form invariant amplitudes.

We finally give the helicity amplitudes in the form that contains the Born-form approximation from refs. [4], [5] given by (2.13), (2.14):

$$\begin{aligned} S_I^{(\sigma)} &= -tY_5^{(\sigma)}, \\ S_Q^{(\sigma)} &= -\frac{ts}{M_Z^2}Y_5^{(\sigma)} + \frac{s(s - M_Z^2)}{M_Z^2}[Y_1^{(\sigma)} + \frac{1}{2}Y_2^{(\sigma)} - \frac{1}{2}Y_3^{(\sigma)} - \sigma\frac{1}{2M_W^2}\cos\theta Y_4^{(\sigma)}] \\ &= \frac{g^2 s}{2M_Z^2}(\delta_{\sigma,-} + \delta_t^{(\sigma)}) \end{aligned} \quad (\text{A.12})$$

$$\begin{aligned}
& + \frac{s(s - M_Z^2)}{M_Z^2} \left[-e^2 \frac{1}{s} \left(1 + \delta_\gamma + \frac{1}{2} (x_\gamma - y_\gamma - \sigma \cos \theta \frac{s}{M_W^2} z_\gamma) \right) \right. \\
& \left. + \left(e^2 - \frac{g^2}{2} \delta_{\sigma,-} \right) \frac{1}{s - M_Z^2} \left\{ 1 + \frac{s_W}{c_W} \left(\delta_Z + \frac{1}{2} (x_Z - y_Z - \sigma \cos \theta \frac{s}{M_W^2} z_Z) \right) \right\} \right], \quad (\text{A.13})
\end{aligned}$$

with $S_i^{(\sigma)}$ ($i = 3, 4, 5, 6$) from (A.4)–(A.7) and

$$\mathcal{M}_3 = \frac{1}{s} \bar{M}_2 - \frac{s - M_Z^2}{2M_Z^2} \mathcal{M}_Q = \frac{1}{s} \bar{M}_2 - \frac{1}{2s} \bar{M}_1, \quad (\text{A.14})$$

$$\mathcal{M}_4 = \frac{1}{s} \bar{M}_3 + \frac{s - M_Z^2}{2M_Z^2} \mathcal{M}_Q = \frac{1}{s} \bar{M}_3 + \frac{1}{2s} \bar{M}_1, \quad (\text{A.15})$$

$$\mathcal{M}_5 = \frac{1}{s} \bar{M}_4 + \frac{s - M_Z^2}{2M_Z^2} \sigma \cos \theta \frac{s}{M_W^2} \mathcal{M}_Q = \frac{1}{s} \bar{M}_4 + \frac{1}{2M_W^2} \sigma \cos \theta \bar{M}_1, \quad (\text{A.16})$$

$$\mathcal{M}_6 = \frac{1}{s} \bar{M}_6. \quad (\text{A.17})$$

Appendix B. Numerical Results in Different Born-Form Approximations

In this appendix we compare the numerical one-loop results for cross sections in the different Born-form approximations based on (2.10), (2.11) and on (2.13), (2.14). The numerical results were obtained by employing the computer code from ref. [14]. Soft-photon bremsstrahlung is included as described in sections 3 to 5. The purpose of this investigation is twofold:

i) to show that the form (2.10), (2.11) for $S_I^{(-)}(s, t)$ and $S_Q^{(\pm)}(s, t)$ yields particularly good results in the high-energy limit, and

ii) to establish the connection with previous work, based on the form (2.13), (2.14).

The results for the differential cross sections at $\sqrt{s} = 2000$ GeV, $\sqrt{s} = 500$ GeV and $\sqrt{s} = 200$ GeV are shown in tables B1, B2 and B3. One observes that the cross section with summation over W^+ and W^- spins and the cross section for production of purely longitudinal W -bosons in the high-energy limit ($\sqrt{s} \cong 2000$ GeV) are better approximated in the Born-form approximation of the present paper, based on $S_I^{(-)}(s, t)$ and $S_Q^{(\pm)}(s, t)$ from (2.10), (2.11).

Angle ($^\circ$)	Born-form approx.		Born-form approx. ([4],[5])		Full one-loop $\frac{d\sigma}{d\cos\theta}$ (pb)	Born $\frac{d\sigma}{d\cos\theta}$ (pb)
	$\frac{d\sigma}{d\cos\theta}$ (pb)	Δ (%)	$\frac{d\sigma}{d\cos\theta}$ (pb)	Δ (%)		
$\sigma^{\text{“unpol”}}$						
10	3.751	+0.02	3.752	+0.04	3.750	5.329
30	2.599×10^{-1}	+0.26	2.604×10^{-1}	+0.36	2.586×10^{-1}	5.070×10^{-1}
50	5.551×10^{-2}	+0.37	5.602×10^{-2}	+0.74	5.500×10^{-2}	1.382×10^{-1}
70	1.727×10^{-2}	+0.21	1.758×10^{-2}	+0.81	1.716×10^{-2}	5.208×10^{-2}
90	7.565×10^{-3}	-0.10	7.597×10^{-3}	+0.02	7.592×10^{-3}	2.605×10^{-2}
110	4.074×10^{-3}	-0.38	3.898×10^{-3}	-1.48	4.135×10^{-3}	1.599×10^{-2}
130	2.007×10^{-3}	-0.49	1.788×10^{-3}	-2.80	2.053×10^{-3}	9.466×10^{-3}
150	6.589×10^{-4}	-0.22	5.319×10^{-4}	-3.40	6.678×10^{-4}	3.993×10^{-3}
170	7.567×10^{-5}	+1.76	5.133×10^{-5}	-2.33	6.520×10^{-5}	5.961×10^{-4}
σ_T						
10	3.751	+0.04	3.751	+0.04	3.749	5.329
30	2.585×10^{-1}	+0.30	2.585×10^{-1}	+0.30	2.570×10^{-1}	5.050×10^{-1}
50	5.330×10^{-2}	+0.45	5.330×10^{-2}	+0.45	5.270×10^{-2}	1.347×10^{-1}
70	1.454×10^{-2}	+0.36	1.454×10^{-2}	+0.36	1.437×10^{-2}	4.720×10^{-2}
90	4.875×10^{-3}	-0.00	4.875×10^{-3}	-0.00	4.876×10^{-3}	2.072×10^{-2}
110	1.956×10^{-3}	-0.48	1.956×10^{-3}	-0.48	2.010×10^{-3}	1.135×10^{-2}
130	7.400×10^{-4}	-0.80	7.400×10^{-4}	-0.80	7.907×10^{-4}	6.367×10^{-3}
150	1.689×10^{-4}	-0.76	1.689×10^{-4}	-0.76	1.887×10^{-4}	2.603×10^{-3}
170	5.448×10^{-6}	-0.26	5.447×10^{-6}	-0.26	6.262×10^{-6}	3.124×10^{-4}
σ_L						
10	4.329×10^{-5}	0.00	9.403×10^{-5}	+124.24	4.329×10^{-5}	4.084×10^{-5}
30	8.894×10^{-4}	0.00	1.315×10^{-3}	+37.14	8.894×10^{-4}	1.146×10^{-3}
50	1.915×10^{-3}	0.00	2.395×10^{-3}	+16.46	1.915×10^{-3}	2.917×10^{-3}
70	2.580×10^{-3}	0.00	2.883×10^{-3}	+6.75	2.580×10^{-3}	4.487×10^{-3}
90	2.625×10^{-3}	0.00	2.656×10^{-3}	+0.60	2.625×10^{-3}	5.126×10^{-3}
110	2.085×10^{-3}	0.00	1.911×10^{-3}	-3.83	2.085×10^{-3}	4.546×10^{-3}
130	1.236×10^{-3}	0.00	1.021×10^{-3}	-7.10	1.236×10^{-3}	3.028×10^{-3}
150	4.528×10^{-4}	+0.01	3.349×10^{-4}	-9.12	4.527×10^{-4}	1.292×10^{-4}
170	3.834×10^{-5}	-0.04	2.499×10^{-5}	-8.60	3.840×10^{-5}	1.559×10^{-4}
σ_{mixed}						
10	6.425×10^{-4}	-39.22	9.313×10^{-4}	-4.15	9.655×10^{-4}	8.236×10^{-4}
30	4.946×10^{-4}	-19.68	5.968×10^{-4}	-7.58	6.608×10^{-4}	8.444×10^{-4}
50	2.959×10^{-4}	-14.97	3.301×10^{-4}	-9.58	3.907×10^{-4}	6.332×10^{-4}
70	1.500×10^{-4}	-13.65	1.583×10^{-4}	-11.54	2.037×10^{-4}	3.933×10^{-4}
90	6.528×10^{-5}	-13.12	6.567×10^{-5}	-12.92	9.151×10^{-5}	1.999×10^{-4}
110	3.252×10^{-5}	-10.57	3.088×10^{-5}	-9.91	4.010×10^{-5}	9.307×10^{-5}
130	3.082×10^{-5}	+6.10	2.637×10^{-5}	-0.17	2.649×10^{-5}	7.099×10^{-5}
150	3.723×10^{-5}	+11.05	2.808×10^{-5}	+1.73	2.638×10^{-5}	9.818×10^{-5}
170	3.188×10^{-5}	+8.87	2.089×10^{-5}	+0.27	2.054×10^{-5}	1.278×10^{-4}

Table B1. The differential cross section $\frac{d\sigma}{d\cos\theta}$ and the deviations from the full one-loop result are shown at $\sqrt{s} = 2000$ GeV, when summing over W polarizations, for transversely polarized W , longitudinally polarized W , and the mixed case. The first column shows the result of the Born-form approximation based on the one-loop evaluation of $S_I^{(-)}$ and $S_Q^{(\pm)}$ given by (2.10) and (2.11). The second column gives the result of previous work [4], [5], which is based on the one-loop evaluation of $S_I^{(-)}$ and $S_Q^{(\pm)}$ given by (2.13), (2.14). The third and fourth columns give the full one-loop results and the Born approximation.

Angle ($^\circ$)	Born-form approx.		Born-form approx. ([4],[5])		Full one-loop $\frac{d\sigma}{d\cos\theta}$ (pb)	Born $\frac{d\sigma}{d\cos\theta}$ (pb)
	$\frac{d\sigma}{d\cos\theta}$ (pb)	Δ (%)	$\frac{d\sigma}{d\cos\theta}$ (pb)	Δ (%)		
	$\sigma^{\text{"unpol"}}$					
10	6.164×10^1	+0.01	6.163×10^1	+0.00	6.163×10^1	7.502×10^1
30	6.524	-0.07	6.529	-0.01	6.530	8.495
50	1.740	-0.25	1.745	-0.04	1.746	2.432
70	6.474×10^{-1}	-0.41	6.509×10^{-1}	-0.04	6.513×10^{-1}	9.578×10^{-1}
90	3.158×10^{-1}	-0.41	3.169×10^{-1}	-0.18	3.178×10^{-1}	4.868×10^{-1}
110	1.861×10^{-1}	-0.30	1.852×10^{-1}	-0.61	1.870×10^{-1}	2.974×10^{-1}
130	1.099×10^{-1}	-0.05	1.083×10^{-1}	-0.93	1.100×10^{-1}	1.824×10^{-1}
150	5.507×10^{-2}	+0.58	5.374×10^{-2}	-0.83	5.452×10^{-2}	9.418×10^{-2}
170	2.434×10^{-2}	+1.55	2.359×10^{-2}	-0.24	2.369×10^{-2}	4.182×10^{-2}
	σ_T					
10	6.128×10^1	+0.00	6.128×10^1	+0.00	6.128×10^1	7.457×10^1
30	6.390	+0.00	6.389	+0.00	6.389	8.329
50	1.600	+0.00	1.600	+0.00	1.600	2.250
70	5.232×10^{-1}	-0.02	5.232×10^{-1}	-0.02	5.234×10^{-1}	7.915×10^{-1}
90	2.149×10^{-1}	-0.03	2.149×10^{-1}	-0.03	2.150×10^{-1}	3.484×10^{-1}
110	1.105×10^{-1}	-0.26	1.105×10^{-1}	-0.26	1.110×10^{-1}	1.914×10^{-1}
130	5.835×10^{-2}	-0.54	5.834×10^{-2}	-0.54	5.893×10^{-2}	1.077×10^{-1}
150	2.251×10^{-2}	-0.54	2.250×10^{-2}	-0.54	2.274×10^{-2}	4.408×10^{-2}
170	2.561×10^{-3}	-0.21	2.560×10^{-3}	-0.21	2.571×10^{-3}	5.293×10^{-3}
	σ_L					
10	1.435×10^{-1}	0.00	1.407×10^{-1}	-1.58	1.435×10^{-1}	1.772×10^{-1}
30	3.309×10^{-3}	0.00	3.098×10^{-3}	-6.03	3.309×10^{-3}	3.497×10^{-3}
50	2.599×10^{-2}	0.00	2.823×10^{-2}	+7.81	2.599×10^{-2}	2.869×10^{-2}
70	5.375×10^{-2}	0.00	5.619×10^{-2}	+3.73	5.375×10^{-2}	6.543×10^{-2}
90	6.634×10^{-2}	0.00	6.728×10^{-2}	+1.09	6.634×10^{-2}	8.630×10^{-2}
110	5.939×10^{-2}	0.00	5.872×10^{-2}	-0.82	5.939×10^{-2}	8.185×10^{-2}
130	3.866×10^{-2}	-0.02	3.748×10^{-2}	-2.11	3.867×10^{-2}	5.647×10^{-2}
150	1.570×10^{-2}	-0.04	1.509×10^{-2}	-2.53	1.571×10^{-2}	2.454×10^{-2}
170	1.763×10^{-3}	-0.01	1.704×10^{-3}	-2.08	1.766×10^{-3}	2.986×10^{-3}
	σ_{mixed}					
10	2.158×10^{-1}	+3.94	2.052×10^{-1}	+0.04	2.051×10^{-1}	2.714×10^{-1}
30	1.310×10^{-1}	-4.31	1.363×10^{-1}	-1.05	1.380×10^{-1}	1.625×10^{-1}
50	1.144×10^{-1}	-3.85	1.175×10^{-1}	-1.83	1.203×10^{-1}	1.531×10^{-1}
70	7.041×10^{-2}	-3.69	7.147×10^{-2}	-2.64	7.413×10^{-2}	1.008×10^{-1}
90	3.462×10^{-2}	-3.53	3.480×10^{-2}	-3.18	3.646×10^{-2}	5.216×10^{-2}
110	1.616×10^{-2}	-1.78	1.604×10^{-2}	-2.28	1.659×10^{-2}	2.414×10^{-2}
130	1.286×10^{-2}	+2.41	1.246×10^{-2}	+0.22	1.242×10^{-2}	1.825×10^{-2}
150	1.686×10^{-2}	+3.09	1.615×10^{-2}	+0.31	1.607×10^{-2}	2.556×10^{-2}
170	2.002×10^{-2}	+2.00	1.932×10^{-2}	-0.09	1.935×10^{-2}	3.355×10^{-2}

Table B2. Same as table B1, but for $\sqrt{s} = 500$ GeV.

Angle ($^{\circ}$)	Born-form approx.		Born-form approx. ([4],[5])		Full one-loop $\frac{d\sigma}{d\cos\theta}$ (pb)	Born $\frac{d\sigma}{d\cos\theta}$ (pb)
	$\frac{d\sigma}{d\cos\theta}$ (pb)	Δ (%)	$\frac{d\sigma}{d\cos\theta}$ (pb)	Δ (%)		
	$\sigma^{\text{"unpol"}}$					
10	3.408×10^1	-0.12	3.413×10^1	0.00	3.413×10^1	4.141×10^1
30	2.310×10^1	-0.04	2.311×10^1	0.00	2.311×10^1	2.813×10^1
50	1.255×10^1	-0.06	1.255×10^1	-0.06	1.256×10^1	1.540×10^1
70	6.958	-0.05	6.960	-0.02	6.962	8.617
90	4.197	-0.04	4.200	+0.02	4.199	5.251
110	2.766	-0.06	2.768	0.00	2.768	3.494
130	1.964	-0.08	1.965	-0.04	1.966	2.502
150	1.502	-0.16	1.503	-0.10	1.505	1.927
170	1.283	-0.18	1.284	-0.10	1.286	1.652
	σ_T					
10	7.998	+0.00	7.999	+0.01	7.998	9.644
30	1.828×10^1	+0.00	1.828×10^1	+0.00	1.828×10^1	2.218×10^1
50	9.977	-0.08	9.977	-0.08	9.987	1.225×10^1
70	4.364	-0.13	4.364	-0.13	4.371	5.432
90	2.166	+0.00	2.166	+0.00	2.166	2.735
110	1.349	+0.06	1.349	+0.06	1.348	1.728
130	8.329×10^{-1}	-0.04	8.330×10^{-1}	-0.03	8.333×10^{-1}	1.083
150	3.576×10^{-1}	-0.11	3.576×10^{-1}	-0.11	3.581×10^{-1}	4.710×10^{-1}
170	4.370×10^{-2}	-0.14	4.370×10^{-2}	-0.14	4.378×10^{-2}	5.801×10^{-2}
	σ_L					
10	1.377	+0.00	1.379	+0.12	1.377	1.671
30	2.325	+0.00	2.328	+0.11	2.325	2.856
50	4.886×10^{-1}	+0.06	4.880×10^{-1}	-0.03	4.882×10^{-1}	6.176×10^{-1}
70	4.896×10^{-2}	+0.20	4.910×10^{-2}	+0.47	4.886×10^{-2}	5.087×10^{-2}
90	3.791×10^{-1}	-0.09	3.807×10^{-1}	+0.27	3.795×10^{-1}	4.495×10^{-1}
110	6.471×10^{-1}	-0.11	6.483×10^{-1}	+0.04	6.480×10^{-1}	7.971×10^{-1}
130	5.735×10^{-1}	-0.12	5.739×10^{-1}	-0.07	5.744×10^{-1}	7.229×10^{-1}
150	2.799×10^{-1}	-0.11	2.800×10^{-1}	-0.08	2.803×10^{-1}	3.588×10^{-1}
170	3.567×10^{-2}	-0.13	3.568×10^{-2}	-0.11	3.573×10^{-2}	4.616×10^{-2}
	σ_{mixed}					
10	2.470×10^1	-0.20	2.475×10^1	+0.03	2.476×10^1	3.010×10^1
30	2.495	-0.16	2.500	+0.00	2.500	3.088
50	2.087	+0.28	2.087	+0.28	2.080	2.532
70	2.545	+0.10	2.546	+0.13	2.542	3.134
90	1.652	-0.05	1.653	+0.00	1.653	2.066
110	7.697×10^{-1}	-0.20	7.704×10^{-1}	-0.12	7.716×10^{-1}	9.685×10^{-1}
130	5.572×10^{-1}	-0.17	5.576×10^{-1}	-0.11	5.584×10^{-1}	6.958×10^{-1}
150	8.648×10^{-1}	-0.16	8.652×10^{-1}	-0.13	8.666×10^{-1}	1.097
170	1.204	-0.19	1.204	-0.19	1.207	1.548

Table B3. Same as table B1, but for $\sqrt{s} = 200$ GeV.

Appendix C. The One-Loop Cross Sections in the High-Energy Approximation

In this appendix, we give the formulae for cross sections in the Born-form high-energy approximation and derive the linear relationship (3.11) to (3.13) between the Born-form invariant amplitudes $\hat{S}_I^{(-)}(s, t)$ and $\hat{S}_Q^{(\pm)}(s, t)$ on the one hand and the cross-section coefficients $C_{-,T}(s, t)$ and $C_{\pm,L}(s, t)$ from ref. [12] on the other hand.

The differential cross section for given helicities σ , λ and $\bar{\lambda}$ is given by

$$\frac{d\sigma(\sigma, \lambda, \bar{\lambda})}{d\cos\theta} = \frac{\pi\beta}{2s^3}\alpha^2|\mathcal{H}(\sigma, \lambda, \bar{\lambda})|^2, \quad (\text{C.1})$$

where the helicity amplitudes in the Born-form approximation become

$$\mathcal{H}(\sigma, \lambda, \bar{\lambda}) = S_I^{(\sigma)}(s, t)\mathcal{M}_I(\sigma, \lambda, \bar{\lambda})\delta_{\sigma,-} + S_Q^{(\sigma)}(s, t)\mathcal{M}_Q(\sigma, \lambda, \bar{\lambda}). \quad (\text{C.2})$$

For longitudinal W -bosons, with our choice of basic matrix elements \mathcal{M}_i given in (A.1) to (A.11), the cross section depends on $S_I^{(\pm)}(s, t)$ and $S_Q^{(\pm)}(s, t)$ only, i.e. relation (C.2) becomes exact for $\sigma = -1$, $\lambda = \bar{\lambda} = 0$ rather than being an approximation. Upon factorization into Born cross section and correction term, for longitudinal W polarization we have

$$\left. \frac{d\sigma}{d\Omega} \right|_{\sigma,L} = \left. \frac{d\sigma}{d\Omega} \right|_{\sigma,L}^{Born} \cdot \left| 1 + \frac{\frac{1}{2s_W^2}\mathcal{M}_I(\sigma, 0, 0)\delta\hat{S}_I^{(\sigma)} + \mathcal{M}_Q(\sigma, 0, 0)\delta\hat{S}_Q^{(\sigma)}}{\frac{1}{2s_W^2}\mathcal{M}_I(\sigma, 0, 0)\delta_{\sigma,-} + \mathcal{M}_Q(\sigma, 0, 0)} \right|^2, \quad (\text{C.3})$$

where $\delta\hat{S}_I^{(\sigma)}(s, t)$ and $\delta\hat{S}_Q^{(\sigma)}$ denote the deviations from their respective Born values:

$$\begin{aligned} \delta\hat{S}_I^{(-)} &= \hat{S}_I^{(-)} - 1, \\ \delta\hat{S}_I^{(+)} &\equiv \frac{1}{2s_W^2}S_I^{(+)}, \\ \delta S_Q^{\pm} &= \hat{S}_Q^{(\pm)} - 1. \end{aligned} \quad (\text{C.4})$$

We stress that (C.3) does not yet involve any approximation. Expanding the coefficients \mathcal{M}_I and \mathcal{M}_Q in powers of s , the cross section (C.3) becomes

$$\left. \frac{d\sigma}{d\Omega} \right|_{-,L} = \left. \frac{d\sigma}{d\Omega} \right|_{-,L}^{Born} \cdot \left| 1 + (2c_W^2 - 1)(1 + O(\frac{1}{s}))\delta\hat{S}_I^{(-)} + 2s_W^2(1 + O(\frac{1}{s}))\delta\hat{S}_Q^{(-)} \right|^2 \quad (\text{C.5})$$

$$\left. \frac{d\sigma}{d\Omega} \right|_{+,L} = \left. \frac{d\sigma}{d\Omega} \right|_{+,L}^{Born} \cdot \left| 1 + \frac{2c_W^2 - 1}{2s_W^2}(1 + O(\frac{1}{s}))\delta\hat{S}_I^{(+)} + \delta\hat{S}_Q^{(+)} \right|^2. \quad (\text{C.6})$$

A high-energy expansion for the production cross section at the one-loop order was derived in ref. [12]. It is given by

$$\left. \frac{d\sigma}{d\Omega} \right|_{-,L} = \left. \frac{d\sigma}{d\Omega} \right|_{-,L}^{Born} \cdot [1 + C_{-,L}^B + C_{-,L}^F], \quad (\text{C.7})$$

$$\left. \frac{d\sigma}{d\Omega} \right|_{+,L} = \left. \frac{d\sigma}{d\Omega} \right|_{+,L}^{Born} \cdot [1 + C_{+,L}^B + C_{+,L}^F]. \quad (\text{C.8})$$

Comparison of (C.5), (C.6) with (C.7), (C.8) yields relations (3.11) and (3.12).

In the case of transverse polarization for the W -bosons, in contradistinction with (C.3), the cross section also contains contributions from invariant amplitudes different from $S_I^{(\pm)}(s, t)$ and $S_Q^{(\pm)}(s, t)$. In this case, (C.2) is indeed an approximation, even for left-handed electrons, $\sigma = -1$. From the numerical one-loop evaluation of appendix B we know that it is an excellent one, i.e. all leading terms are taken into account by this high-energy Born-form approximation. Moreover, according to table A1, equal transverse helicities are suppressed in contrast with opposite ones for which \mathcal{M}_Q is suppressed. The one-loop corrected cross section at high energies for transverse polarization of the W bosons depends on $\hat{S}_I^{(-)}(s, t)$ only:

$$\left. \frac{d\sigma}{d\Omega} \right|_{-,T} = \left. \frac{d\sigma}{d\Omega} \right|_{-,T}^{Born} \cdot |1 + \delta \hat{S}_I^{(-)}|^2. \quad (\text{C.9})$$

Comparison with ref. [12],

$$\left. \frac{d\sigma}{d\Omega} \right|_{-,T} = \left. \frac{d\sigma}{d\Omega} \right|_{-,T}^{Born} \cdot [1 + C_{-,T}^B + C_{-,T}^F], \quad (\text{C.10})$$

immediately implies relation (3.13).

In summary, with our choice of basic matrix elements, the high-energy one-loop correction coefficients to cross sections, originally introduced without reference to a Born-form approximation, become identical to linear combinations of Born-form invariant amplitudes.

References

- [1] M. Lemoine and M. Veltman, *Nucl. Phys.* **B164** (1980) 445.
- [2] J. Fleischer, F. Jegerlehner and M. Zralek, *Z. Phys.* **C42** (1989) 409.
- [3] M. Böhm, A. Denner, T. Sack, W. Beenakker, F.A. Berends and H. Knijf, *Nucl. Phys.* **B304** (1988) 463.
- [4] J. Fleischer, J.L. Kneur, K. Kolodziej, M. Kuroda and D. Schildknecht, *Nucl. Phys.* **B378** (1992) 443; Erratum, *ibid.* **B426** (1994) 246.
- [5] S. Dittmaier, M. Böhm and A. Denner, *Nucl. Phys.* **B376** (1992) 29; Erratum, *ibid.* **B391** (1993) 483.
- [6] S. Dittmaier, *Acta Phys. Pol.* **B28** (1997) 619, talk given at the Cracow International Symposium on Radiative Corrections to the Standard Model, Cracow, 1996.
- [7] S. Dittmaier, CERN-TH/97-302, hep-ph/9710542, talk given at the International Europhysics Conference on High-Energy Physics, Jerusalem, 1997.
- [8] W. Beenakker and F.A. Berends, in *Physics at LEP2*, eds. G. Altarelli et al. (CERN 96-01, Geneva, 1996), Vol.I, p. 79.
- [9] M. Kuroda, I. Kuss and D. Schildknecht, *Phys. Lett.* **B409** (1997) 405.
- [10] S. Dittmaier, D. Schildknecht and G. Weiglein, *Nucl. Phys.* **B465** (1996) 3.
- [11] M. Bilenky, J.L. Kneur, F.M. Renard and D. Schildknecht, *Nucl. Phys.* **B409** (1993) 22.
- [12] W. Beenakker, A. Denner, S. Dittmaier, R. Mertig and T. Sack, *Nucl. Phys.* **B410** (1993) 245; W. Beenakker, A. Denner, S. Dittmaier and R. Mertig, *Phys. Lett.* **B317** (1993) 622.
- [13] Y.Y. Kim, talk given at the 18th International Symposium on Lepton-Photon Interactions, DESY, Hamburg, 1997.
- [14] M. Kuroda, Analytic expression of the radiative corrections to the process $e^+e^- \rightarrow W^+W^-$ in one-loop order, 1994, unpublished.